Candida Cell Heterogeneity Measured With a Microwave Flow Cytometer

Neelima Dahal, Carl Ehrett, Jeffrey A. Osterberg, Ralu Divan, and Pingshan Wang, *Senior Member, IEEE*

***Abstract*—Heterogeneity is an important property of a cell population. It is an intrinsic driving force behind biological evolution and a main challenge for effective disease treatment, such as precision solid cancer therapy. Various "omics" methods, mass spectroscopy-based techniques, and flow cytometry have been developed for cell heterogeneity characterization. But current methods are either low throughput or invasive. In this work, we develop a simple microwave flow cytometer to measure single *C. tropicalis* and *C. albicans*, which are two of the most important *Candida* yeasts that cause candidemia disease. The obtained scatter plots of cell permittivity for both the species show a colinear relationship for cells of different volumes, which indicates a largely conserved cell molecular composition profile despite heterogeneous cell sizes. We also apply microwave flow cytometer to measure antifungal drug effect on *C. tropicalis* and *C. albicans* cell population and observe that drugs induce significant heterogeneity increase. The results show that microwave flow cytometry is a promising new method for high throughput and noninvasive characterization of cell heterogeneity. More work is needed, including the determination of biological significance of the observed microwave heterogeneity.**

***Index Terms*—Cell heterogeneity, microwave sensing, permittivity, *candida yeast*, flow cytometry.**

I. Introduction

HETEROGENEITY is a fundamental property of biological cells that contributes to cell development [1], differentiation [2], tumorigenesis [3], and immune mediated responses [4], among others. Understanding heterogeneity is one of the greatest challenges of drug discovery since seemingly identical cells can respond differently to drugs for disease treatment [5]. For advanced cell therapy products, such as those based on mesenchymal stromal cells (MSCs), heterogeneity pervades at multiple levels, from sample source to single cell [6]. Cellular heterogeneity is also the main challenge in treating solid tumors, such as colorectal cancer [7], breast cancer [8], hepatocellular carcinoma [9], and lung cancer [10]. On the other hand, cell heterogeneity, which is sometimes referred to as noise, can provide information that is important for a wide range of applications. For instance, intratumor heterogeneity (ITH) was shown as a prognostic predictor to predict the risk of recurrence of non–small-cell lung cancer [11].

Heterogeneity comes from genetic variation and nongenetic characteristics [12]. Nongenetic variation, also known as phenotypic heterogeneity, describes variations that are observed between individual cells in a genetically homogeneous population [13]. The differences of cellular constituents, including DNA, proteins, RNA, lipids, carbohydrates, and metabolites, yield heterogeneous cell properties and functions. No two cells are identical and cellular heterogeneity is universal, including in isogenic or a clonal population of cells [14]. Therefore, measuring and understanding cell heterogeneity at different scales are important. Microscopes have been used for cell size and shape characterization. Various molecular approaches have been developed to characterize cell heterogeneity or profile [4] at molecular levels. Single cell "omics," such as DNA sequencing, proteomics, metabolomics, epigenomics, and transcriptomics, examines single molecules but is invasive, complicated and at low throughput. So are mass spectroscopy-based methods, which enable the detection of highly multiplexed analytes in single cells. High content screening, digital pathology, and flow cytometry are high throughput but require labels. Therefore, new, high throughput, and noninvasive methods for cell heterogeneity characterization, classification and studies are of great interest.

Microwave fields can probe cell organelles [15], and have been demonstrated for single cell measurement, such as Chinese hamster ovary cells (CHO) [16], human monocytes THP1 cells [17], Jurkat cell [18], and baker's yeast cells [19]. The measurements are accurate, label-free and non-invasive. In this work, we show that accurate, quantitative and high-throughput microwave dielectric spectroscopy is promising to be a new method for cell heterogeneity characterization. We also report cell size quantification using microscopy cell imaging to further assist cell heterogeneity study.

II. Experimental Setup

A. Microwave Flow Cytometer

Fig. 1(a) shows a schematic of the microwave flow cytometer used in this study. It uses a vector network analyzer (VNA) for

Manuscript received 30 September 2022; revised 23 December 2022; accepted 13 January 2023. Date of publication 2 February 2023; date of current version 31 May 2023. This work was supported in part by the US Army Office of Research under Contract W911NF2210044, in part by the NSF under Grant 1711463, and in part by the U.S. Department of Energy, Office of Science, Office of Basic Energy Sciences under Contract DE-AC02-06CH11357 for the use of the Center for Nanoscale Materials, an Office of Science user facility. *(Corresponding author: Pingshan Wang.)*

Neelima Dahal, Jeffrey A. Osterberg, and Pingshan Wang are with the Holcomb Department of Electrical and Computer Engineering, Clemson University, Clemson, SC 29634 USA (e-mail: ndahal@clemson.edu; josterb@clemson.edu; pwang@clemson.edu).

Carl Ehrett is with the School of Computing, Clemson University, Clemson, SC 29634 USA (e-mail: cehrett@clemson.edu).

Ralu Divan is with the Center for Nanoscale Materials, Argonne National Laboratory, Lemont, IL 60439 USA (e-mail: divan@anl.gov).

Digital Object Identifier 10.1109/JERM.2023.3239557

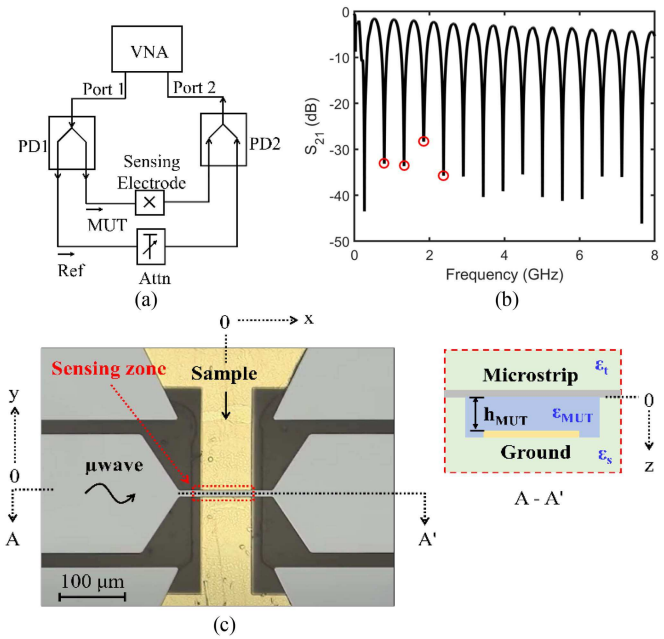

Fig. 1. (a) A schematic of the microwave flow cytometer. Two power dividers, PD1 and PD2 are used. MUT is material-under-test branch and Ref is reference branch. (b) Typical broadband *S21* magnitude (measured). The notch frequencies are measurement frequencies, such as those labelled with red circles. (c) A microscope picture of the microstrip sensing electrode showing microfluidic channel (blue) with height h_{mut} approximately 10 μm and width 100 μm, which is also the microstrip line length l.

probing signal generation and detection with an interferometer to enhance measurement limit-of-detection (LOD). Fig. 1(b) shows a typical broadband S_{21} magnitude, and the measurement is performed at the null points, also known as notch frequencies. The measurement results presented in this paper were measured at the frequency points labelled with red circles because they provide a significant separation between viable and non-viable cells. At higher frequencies, the permittivity difference between viable and non-viable cells decreases, as discussed in [20]. The lowest frequency point measured was 0.796 GHz. Since the measurement presented in this paper was done over a span of time, the change of the interferometer tuning status was considered. The interference nulls were picked at the time of the measurement, and calibration at that exact frequency point was performed within a few hours of measurement. Prior to the next cell measurement, the interference null points were re-evaluated, and measurement was performed at those null points. A simple microstrip line is used as a sensing electrode. Similar systems have been previously reported, such as in [19] and [20]. The VNA power was set at 0 dBm. Broadband measurements show the power loss due to cell sample absorption is much less than 10% (−1 dB plus 3 dB power division). Furthermore, liquid sample is in flow (not static). Therefore, microwave field effects on cells are small and power absorbed by cells is also small. As a result, heating was assumed to be negligible. The cell culture was suspended in de-ionized water stored at room temperature, and the measurement was performed at room temperature. Although slight variation of room temperature is known to occur, calibrating measurement system and carrier medium every few hours minimize potential issues. Furthermore, temperature change is considered a slow process. Thus, for each batch of measurement (e.g., within one hour), less environmental temperature effects are expected. Therefore, temperature effects on cell measurement are neglected. Any ionic effects are assumed to be consistent for all single cell measurements because the cell culture and cell dilution technique used was the same every time. Ionic effect in the drug treated cells is likely of importance but has not been investigated in this paper.

When a cell passes through the microstrip sensing zone and interacts with the probing microwave fields, cell signals are detected and recorded by the VNA. Detailed HFSS (high-frequency structure simulator) simulation analysis shows approximately 6% maximum signal variation when the cell follows different trajectories with slightly nonuniform probing fields [19]. This variation will likely complicate cell heterogeneity analysis.

Cell permittivity values at frequency f, $\varepsilon(f) = \varepsilon'(f)\text{-}j\ \varepsilon''(f)$, are obtained by measuring two calibration fluids, $cal_{1,2}$, carrier liquid, which is culture medium diluted with de-ionized water in a 1:40 ratio, and carrier liquid with a single cell [19]. Any fluids with known $\varepsilon(f)$ can be used as calibration fluids. The obtained scattering parameters are then used to obtain the effective propagation constant, $\gamma = \alpha + j\beta$, of the probing microwave where α is the attenuation constant and β is the phase constant.

$$\gamma_{MUT} l_{MUT} = ln\left[\left(\frac{S_{21MUT} - S_{21cal1}}{S_{21cal2} - S_{21cal1}}\right) \times \left(e^{-\gamma_{cal2} l_{cal2}} - e^{-\gamma_{cal1} l_{cal1}}\right) - e^{-\gamma_{cal1} l_{cal1}}\right] \quad (1)$$

The effective permittivity of the microstrip portion is obtained by use of

$$\varepsilon'_{eff} = \frac{\beta^2 - \alpha^2}{\omega^2 \mu_0 \varepsilon_0}, \varepsilon''_{eff} = \frac{2\alpha\beta}{\omega^2 \mu_0 \varepsilon_0} \quad (2)$$

The effective permittivity assumes a homogeneous medium surrounding the microstrip. Then, the permittivity of MUT, ε_{MUT}, is obtained through a look-up table approach, similar to the one in [19].

B. Sample Preparation

Candida yeast, *C. tropicalis* (ATCC No. 13803) and *C. albicans* (ATCC No. 13804) were purchased from American Type Culture Collection (ATCC) and cultured in YPD (Yeast Extract–Peptone–Dextrose) by following the recommended processes described in [21]. *C. tropicalis* and *C. albicans* were chosen since they are two of the five most important *Candida* yeasts that cause more than 90% of candidemia cases in the US. Single nonbudding *C. tropicalis* and *C. albicans* were easy to choose for microwave measurement due to their round shape. The viable and non-viable cells measured using microwave methods and reported below were also tested using Trypan blue to confirm cell viability. Only a small percentage, <1%, of viable cell sample picked up blue stain confirming >99% cell viability. Agreeable results were obtained for heat-shocked non-viable cells.

Prior to microwave measurement, *Candida* cells were cultured in 50 mL sterile YPD medium in an orbital shaker at 250 rpm and 30 °C overnight (approximately 18 hours). The overnight culture, which would be in stationary phase due to 18 hours of incubation, was transferred to a 1.5 mL centrifuge tube and stored at room temperature while conducting the experiment. Cells were diluted with a ratio of 1:40 in de-ionized water before injecting into the microfluidic channel for measurement. This diluted cell sample was tested with Trypan blue at the end of each microwave measurement to confirm cells remained viable. The sample for drug effect measurement was prepared by first diluting cells in de-ionized water, then pipetting CSP-DMSO into the sample tube, and then gently shaking the tube to thoroughly mix. Measurements began 10 minutes after the drug treatment and lasted for 30 minutes to 1 hour.

III. Microwave Measurement of C. Tropicalis and C. Albicans: Cell Heterogeneity

Viable C. tropicalis and C. albicans samples were prepared and measured at multiple frequencies. The measurement operation can be at a throughput up to ~100-cell/second at a single frequency point. But each batch of measurement can take up to two hours in our cell heterogeneity investigation. For the study presented in Section III, approximately 100 each of single non-budding C. tropicalis and C. albicans cells were measured by transporting each cell back and forth in the sensing zone for 20 seconds. This allowed us to carefully observe, take microscopic image and verify measurement repeatability of each cell by capturing each cell measurement 1–3 times at a given frequency point. For the study presented in Section IV, approximately 100–150 each viable, drug-treated, and non-viable cells were measured where single budding and non-budding cells passed the sensing zone in a continuous flow such that each cell was measured only once. Two C. tropicalis cells, each approximately 7 μm in diameter, where one passed the sensing zone towards the center and the other towards the edge of the microstrip ground, had a 2.7% $\Delta\varepsilon$' and a 0.55% $\Delta\varepsilon$" differences. The results show that wide channels can be used with microstrip sensing electrode for convenient cell transport and accurate cell measurement. System operation stability and repeatability was evaluated in detail and reported in [20].

A. *Measured Permittivity of* C. Tropicalis *and* C. Albicans

Fig. 2(a) and (b) show measured, absolute $\Delta\varepsilon$' and $\Delta\varepsilon$" ($\Delta\varepsilon = \Delta\varepsilon'\text{-}j\Delta\varepsilon'' = \varepsilon_{MUT}\text{-}\varepsilon_{media}$) of viable *C. tropicalis* at 1.32 GHz and 1.85 GHz, respectively. The cells are grouped based on their size with group 1 (blue dashed circle) representing the smallest size and group 4 the largest size. Some cells in each group are also labeled with their images shown. A few observations can be made. First, there is a wide distribution of $\Delta\varepsilon$' and $\Delta\varepsilon$" as shown in Table I where the distribution is calculated as $\Delta\varepsilon'_{distribution} = (\Delta\varepsilon'_{high}\text{-}\Delta\varepsilon'_{median})/\Delta\varepsilon'_{median}$. A maximum $\Delta\varepsilon'_{distribution}$ of 82.2% is seen at 1.85 GHz, and a maximum $\Delta\varepsilon''_{distribution}$ of 84.3% is seen at 1.32 GHz. Thus, cell heterogeneity is high. Second, it seems that $\Delta\varepsilon$' vs $\Delta\varepsilon$" scatter plot follows a linear relationship and cell permittivity aggregates along straight lines,

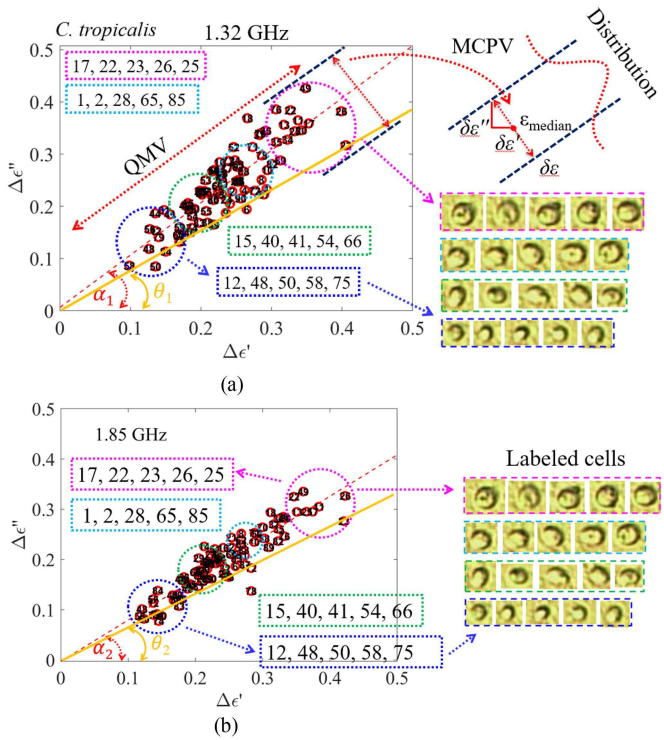

Fig. 2. (a) Measured permittivity of viable *C. tropicalis* at 1.32 GHz and an illustration of QMV and MCPV. For *C. tropicalis*, the MCPV is much smaller than QMV. (b) Measured permittivity of viable *C. tropicalis* at 1.85 GHz.

TABLE I
$\Delta\varepsilon$ Distribution of *C. Tropicalis* at 1.32 and 1.85 GHz

	1.32 GHz	**1.85 GHz**
$\Delta\varepsilon'_{low}$	0.098	0.12
$\Delta\varepsilon'_{high}$	0.41	0.42
$\Delta\varepsilon''_{low}$	0.085	0.078
$\Delta\varepsilon''_{high}$	0.43	0.34
$\Delta\varepsilon_{median}$	0.23 - j0.23	0.23 - j0.19
$\boldsymbol{\Delta\varepsilon'_{distribution}}$	76.4%	**82.2%**
$\boldsymbol{\Delta\varepsilon''_{distribution}}$	**84.3%**	72.9%

i.e., the dashed red lines that pass the origin (0, 0). If we examine each individual cell by drawing a line that connects its ($\Delta\varepsilon$', $\Delta\varepsilon$") and the origin (00), such as cell #23 and the yellow solid line in Fig. 2(a), cell permittivity ($\Delta\varepsilon$', $\Delta\varepsilon$") can be described as (ρ, θ) in a polar coordinate system. A scaled version of cell #23 is expected to have a permittivity value on the yellow line, but at different ρ. If the scaled cell has a zero volume, then its ($\Delta\varepsilon$', $\Delta\varepsilon$") must be at origin (00). Visual observation of cell images in Fig. 2 and preliminary image analysis in Section B below concur with the observation. On the other hand, two *C. tropicalis* cells that have the same ρ but with different θ are likely to have similar size but with different molecular composition since different molecules have different dynamics, such as different $\Delta\varepsilon''/\Delta\varepsilon'$ at a given frequency. Therefore, it is reasonable to assume that ρ and θ indicate cell size or the quantity of molecules (QM) and the overall molecular composition profile (MCP) of a cell, respectively.

Therefore, the red-dashed lines in Fig. 2(a) and (b) likely represent the average permittivity or population property of

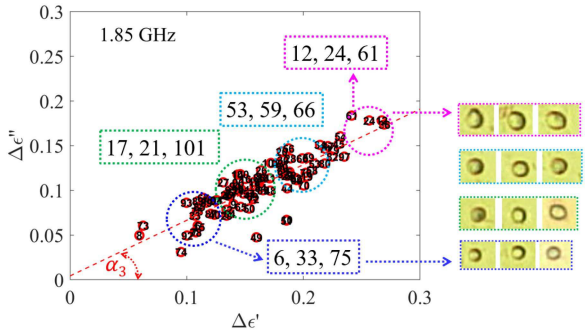

Fig. 3. Measured permittivity of viable *C. albiacns* at 1.85 GHz along with a few selected images. The cells are visually verified as single nonbudding cells.

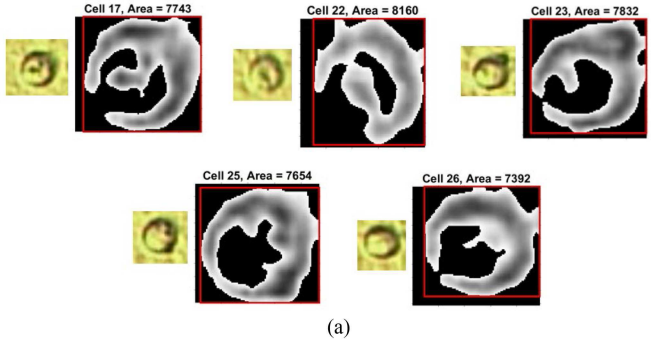

Fig. 4. Cell size estimation by first converting rgb image to gray image, which is then converted into binary image. (a) The area reported here is the area of the box that surrounds the cell image. (b) Further denoising the binary image, and then finding the convex hull of the resulting segmented image.

C. tropicalis. The linear $\Delta\varepsilon$' vs $\Delta\varepsilon$" relationship also suggests that the MCP of *C. tropicalis* cells is largely conserved even when cell sizes are significantly different. Thus, it seems reasonable to separate *C. tropicalis* heterogeneity into QM variation (QMV) and MCP variation (MCPV), as illustrated in Fig. 2(a). Additionally, the distributions of QMV and MCPV, also illustrated in Fig. 2(a), can be modeled and characterized.

Cell permittivity is bounded by two lines such as the two dashed blue lines parallel to the population property line as shown in Fig. 2(a). The distance between the two lines, $2\times\delta\varepsilon$, is an indicator of MCPV. Corresponding projections of $\delta\varepsilon$' and $\delta\varepsilon$" describe the MCPV magnitude, which are much smaller than the 113.8% and 110% QMV for *C. tropicalis* at 1.32 GHz and 1.85 GHz, respectively. QMV is calculated as $\sqrt{\Delta\varepsilon'_{distribution}{}^2 + \Delta\varepsilon''_{distribution}{}^2}$. Cells that are not on the average permittivity lines, such as cell #23, have slightly different MCP, as indicated by the angle θ_1 and θ_2 at 1.32 GHz and 1.85 GHz, respectively. Moreover, (α_1-θ_1) is larger than (α_2-θ_2) indicating frequency dependent MCPV values even though the actual cell MCP is expected to be conserved. Additionally, more detailed examination of Fig. 2(a) shows non-linear contours of cell permittivity distribution. Further examination of Fig. 2 shows that cells in group 1 have slightly larger θ variations than cells in group 4. This might be biologically reasonable since larger cells have more traits in common that enable them to grow larger.

Another example of cell QMV and MCPV is shown in Fig. 3 for *C. albicans* at 1.85 GHz. The variation in $\Delta\varepsilon$' ranges from approximately $\Delta\varepsilon'_{low,1.85GHz} = 0.06$ to $\Delta\varepsilon'_{high,1.85GHz} = 0.27$, and in $\Delta\varepsilon$" from $\Delta\varepsilon''_{low,1.85GHz} = 0.031$ to $\Delta\varepsilon''_{high,1.85GHz} = 0.18$ at 1.85 GHz. The overall distribution in $\Delta\varepsilon$' and $\Delta\varepsilon$" are 70.2% and 75.5%, respectively. It is shown that $\Delta\varepsilon_{min}$ and $\Delta\varepsilon_{\max}$ for nonbudding *C. tropicalis* cell are larger than that of nonbudding *C. albicans* due to larger cell size of *C. tropicalis* cells compared to that of *C. albicans*.

B. Cell Size and Permittivity

To quantify cell sizes, the microscopy images of *Candida* cells shown in Figs. 2 and 3 are examined using MATLAB image processing tool to determine the relative size of each cell. Two independent methods were employed – bounding box method and convex hull method. In the bounding box method, cell size is estimated by computing the area of the box binding the cell image as shown in Fig. 4(a) in which the original microscopy cell image is shown on the left, and the processed image along with the cell number and unitless area is shown on the right. In the convex hull method, only the area inside the convex hull of the segmented cell image is computed to determine the cell size, which is also reported as a unitless area. The convex hull method is thus a more suitable method to estimate cell size. However, due to the low resolution of the microscopy cell image, the convex hull method is not very accurate when the cell outline is not well defined as is the case with cell 22 shown in Fig. 4(b). For the same cell, in the bounding box method, cell area computation considers the entire cell if some cell outline is present in the microscopy cell image. The bounding box method is the most suitable for round shaped cells; same oblong cell with different orientation would otherwise result in different cell area. Since *C. tropicalis* and *C. albicans* are round shaped, we assume that cell orientation has insignificant effect on cell size/area computation using bounding box method.

Shown in Fig. 5(a) and (b) are the normalized (by maximum value) cell area obtained using the bounding box method described above for the cells in the different size groups identified in Fig. 2. The QMV that was hypothesized in the earlier section based on visual cell image comparison is quantified here. The average normalized cell area (0.95) is the largest for group 4 cells, and the smallest (0.49) for group 1 cells. The best fit line is the same as shown in Fig. 2(a) and (b) for 1.32 and 1.85 GHz, respectively. The number overlapping the red marker

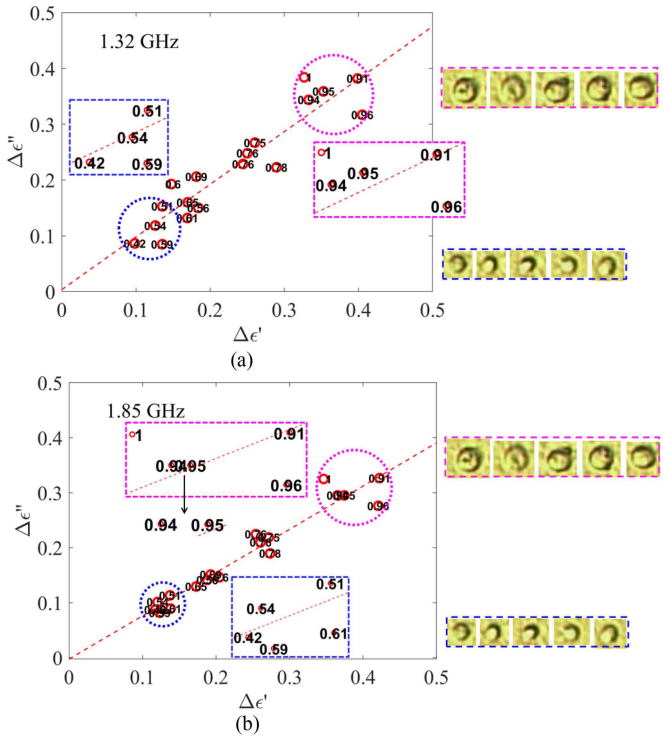

Fig. 5. Measured permittivity of viable *C. tropicalis*, along with the images of the measured cells. The numbers within the plot correspond to the normalized cell area computed using bounding box method. (a) At 1.32 GHz. (b) At 1.85 GHz.

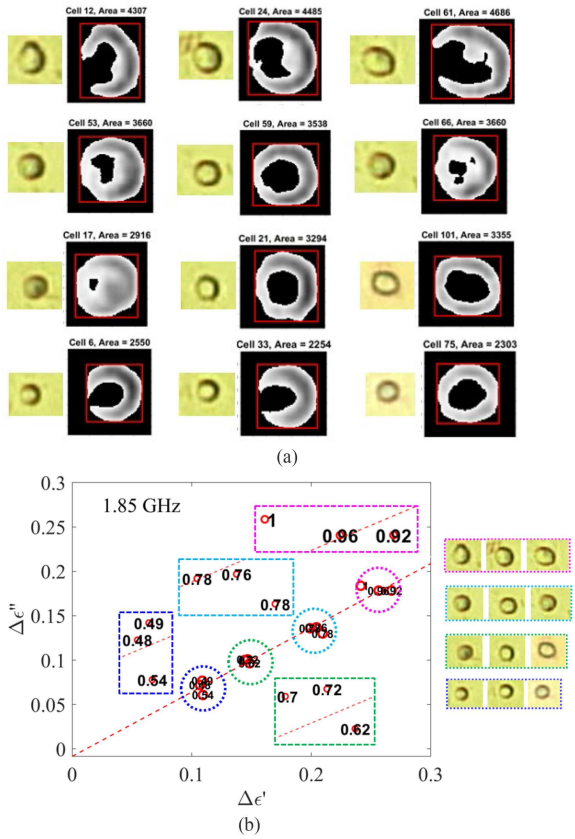

Fig. 6. (a) Cell size estimation by first converting rgb image to gray image, which is then converted into binary image. (b) Measured permittivity of viable *C. albicans* at 1.85 GHz, along with the images of the measured cells. The numbers within the plot correspond to the normalized cell area computed using bounding box method.

in the plot is the corresponding normalized cell area, and only the grouped cell data is shown for clarity. Normalized cell radius (r) was calculated by rearranging the equation for the area of a circle, $A = 4\pi r^2$ where A is the normalized cell area. Then normalized cell volume (V) was approximated using the equation $V = (4/3)\pi r^3$, assuming spherical shaped cells. The largest and the smallest cell volumes were $V_{\max} = 0.094$ and $V_{\min} = 0.0256$, respectively which showed a 114.4% distribution in cell volumes. The corresponding QMV as reported earlier was 113.7% at 1.32 GHz and 110% at 1.85 GHz, which shows a great correlation between the estimated cell volume and measured cell QMV.

Shown in Fig. 6(a) is the cell size analysis of *C. albicans* using the bounding box method. The original microscopy cell image is shown on the left, and the processed image within a bounding box is shown on the right. The larger cells are shown in the top row, and the smaller ones in the bottom. As previously mentioned, the area reported by the bounding box method is unitless and is normalized in Fig. 6(b).

IV. Drug Induced Cell Heterogeneity Change

Antifungal drug called Caspofungin (CSP) diacetate dissolved in dimethyl sulfoxide (DMSO) was used to treat *Candida* cells. Drugs of different doses were used to treat approximately 10^6 cells in 1 mL sample volume. Microwave measurements started 10 minutes after drug application, and 40–60 cells were examined in 30–60 minutes. For CSP, the limited measurement time duration was expected to not cause significant issues as discussed in [20].

Shown in Fig. 7(a) is the cell measurement post CSP treatment compared to the viable and non-viable cells of the same *C. tropicalis* species at 0.796 GHz. The non-viable cells were obtained by heat shocking viable cells at 90 °C for 1 minute. The permittivity measurement of drug treated cell population lies in between the permittivity measurements of viable and non-viable cells, and a larger distribution in permittivity is seen. To analyze the spread of each data group, the data is translated by a small constant (e_1, e_2) so that the resulting polar coordinates ρ and θ (corresponding to the length and width of each group) are de-correlated. This is equivalent to translating the data so that a linear fit of each group intersects the origin. For each group, (e_1, e_2) is found by minimizing the expression (3) below. Having found de-correlated ρ and θ values for each group, we can analyze the length and width of each group.

$$\mathrm{E}\left(\sqrt{(\epsilon_1 - e_1)^2 + \left((\epsilon_2 - e_2)^2\right)}.\tan^{-1}\frac{\epsilon_2 - e_2}{\epsilon_1 - e_1}\right) - \mathrm{E}\left(\sqrt{(\epsilon_1 - e_1)^2 + \left((\epsilon_2 - e_2)^2\right)}\right).\mathrm{E}\left(\tan^{-1}\frac{\epsilon_2 - e_2}{\epsilon_1 - e_1}\right) \tag{3}$$

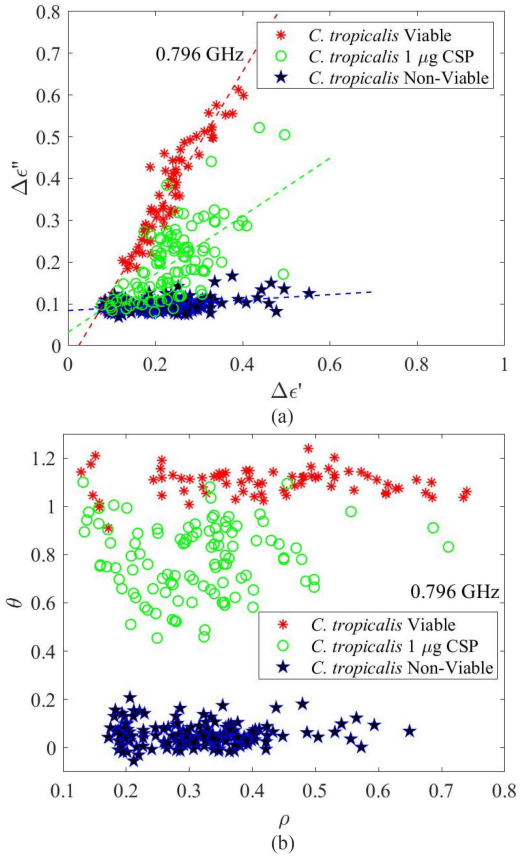

Fig. 7. (a) Microwave measurement of *C. tropicalis* exposed to CSP at 0.796 GHz. (b) Data converted to polar coordinates to analyze ρ and θ of each measurement group namely viable, drug treated, and non-viable *C. tropicalis* cells.

TABLE II
C. TROPICALIS DISTRIBUTION COMPARISON FOR VIABLE, DRUG TREATED, AND NON-VIABLE CELLS

	Viable	CSP	Non-Viable
ρ_{mean}	0.4253	0.3148	0.3133
ρ_{std}	**0.1537**	0.1069	0.0955
θ_{mean}	1.0991	0.7781	0.0554
θ_{std}	0.0535	**0.1512**	0.0455

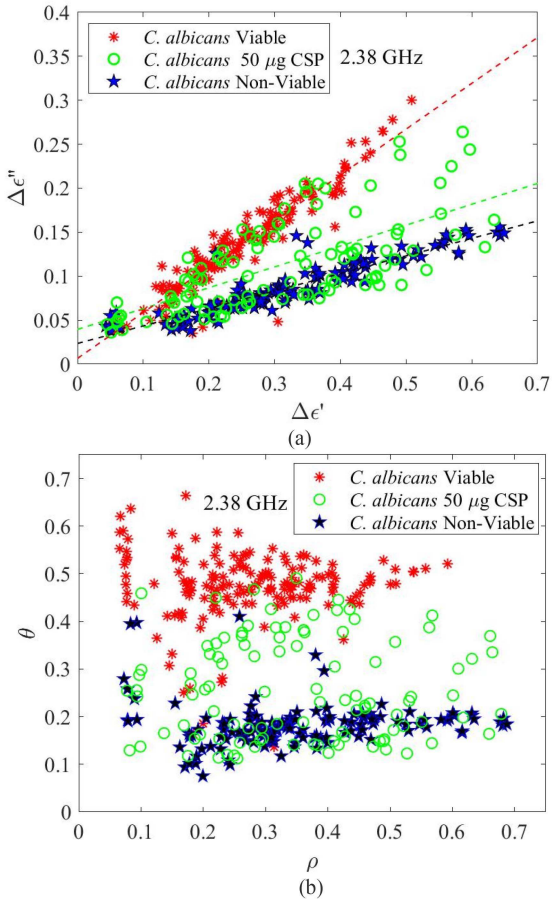

Fig. 8. (a) Microwave measurement of *C. albicans* exposed to CSP at 2.38 GHz. (b) Data converted to polar coordinates to analyze ρ and θ of each measurement group namely viable, drug treated, and non-viable *C. albicans* cells.

TABLE III
C. ALBICANS DISTRIBUTION COMPARISON FOR VIABLE, DRUG TREATED, AND NON-VIABLE CELLS

	Viable	CSP	Non-Viable
ρ_{mean}	0.2773	0.3525	0.3525
ρ_{std}	0.1223	**0.1530**	0.1461
θ_{mean}	0.4740	0.2518	0.1832
θ_{std}	0.0734	**0.1004**	0.0484

Shown in Fig. 7(b) is the data obtained from Fig. 7(a) using polar coordinates as outlined above. The resulting distribution is summarized in Table II. The width (θ) of the CSP treated *C. tropicalis* cells is three times larger than those of viable and non-viable cells. This indicates a large drug-induced cell heterogeneity. Also of interest is the largest length (ρ) of the viable cells, approximately 1.5 times larger than those of CSP treated and non-viable cells. This is likely due to the cell size of the viable population being larger than the other groups. As discussed in [19] and [20], heat shocking permeates cell membrane which reduces the average cell size. Likewise, CSP antifungal effect is due to blockade of the cell wall synthesis [22], and hence produces similar effects as heat shocking.

Shown in Fig. 8(a) is the cell measurement post CSP treatment compared to the viable and non-viable cells of the same species for *C. albicans* at 2.38 GHz. A similar polar coordinate is done and shown in Fig. 8(b). The resulting distribution is summarized in Table III. The width of the CSP treated *C. albicans* cells is approximately 1.4 times and 2 times larger than that of viable and non-viable cells, respectively. Both these factors are smaller than the one observed for *C. tropicalis* drug effect. Thus, drug induced cell heterogeneity occurs at varying degrees for different *Candida* species. The length of the viable, drug-treated, and non-viable cells are similar unlike the case with *C. tropicalis*. *C. albicans* cell wall porosity is significantly lower than that of *C. tropicalis*. Hence a larger concentration of drug, 50 μg per 10^6 cells, is needed for *C. albicans* compared to 1 μg per 10^6 cells for *C. tropicalis* to induce 50% cell death (MIC_{50}). Moreover, the *Candida* cell wall is a very complex structure consisting of many layers, each of which has its own response to CSP. Some of these responses are similar for the two *Candida* species, while others are different which could result in the differences in drug induced cell heterogeneity for *C. tropicalis* and *C. albicans*.

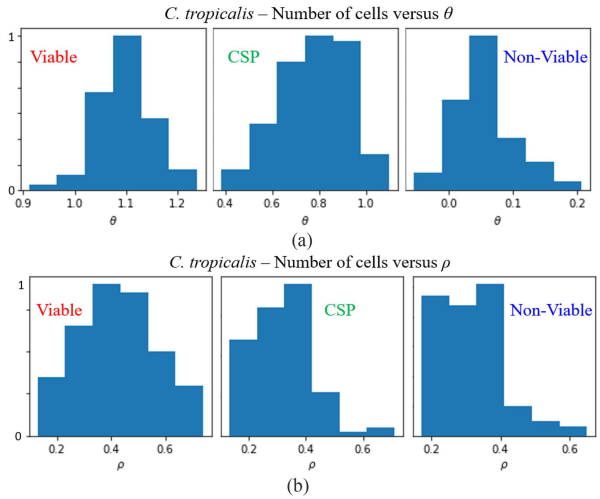

Fig. 9. Histogram of number of cells on the y-axis and (a) θ on the x-axis (b) ρ on the x-axis for *C. tropicalis* viable, CSP treated, and non-viable cells at 0.796 GHz.

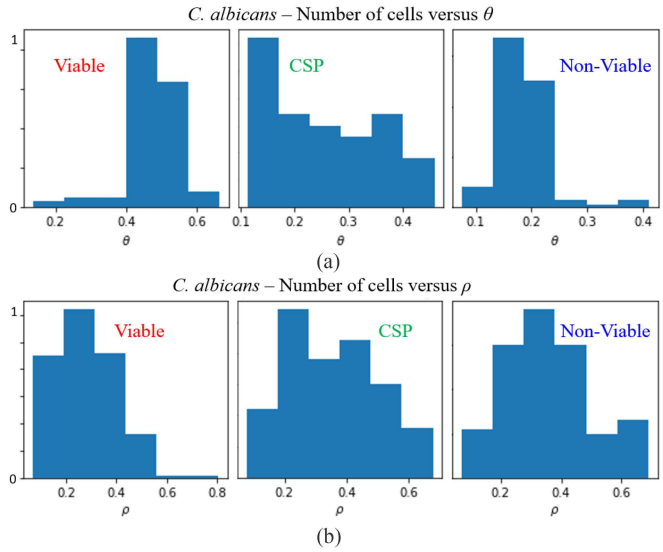

Fig. 10. Histogram of number of cells on the y-axis and (a) θ on the x-axis (b) ρ on the x-axis for *C. albicans* viable, CSP treated, and non-viable cells at 2.38 GHz.

Shown in Fig. 9(a) and (b) are the total number of cells corresponding to a range of ρ and θ values, respectively for viable, drug treated and non-viable *C. tropicalis*. Similar diagrams for *C. albicans* are shown in Fig. 10(a) and (b). Since the number of cells measured for the different groups within each species was not the same, the y-axis is normalized. For *C. tropicalis* cell numbers plotted against ρ, an almost symmetrical distribution is seen for viable cells, and skew right distribution is seen for drug treated and non-viable cells. As discussed previously, ρ represents the QMV implying a normal distribution of cell size of viable population. Both CSP and heat shocking permeate cell membrane, so the skew right distribution of drug treated, and non-viable cells imply a reduction in cell size (i.e., QM) of the general cell population in each group. This reduction in size, however, is only slightly noticeable when microscopic images of cell populations are compared. Since the cell size has a large range [23], individual cells from each group cannot be visibly identified. The MCPV, θ, also has a right skew distribution for non-viable cells and most of these cells have a narrow range of θ. This is due to the permeable cell membrane allowing cell cytoplasm to exchange with the surrounding de-ionized water, thereby reducing the differences in cell molecular composition. The viable cells have an almost symmetrical distribution which is taller and narrower compared to the ρ diagram. This is expected because QMV is larger than MCPV. The drug treated θ diagram shows a tall and wide skew left distribution. The θ diagram of non-viable cells shows a skew right distribution like its ρ diagram counterpart.

The ρ diagram of viable *C. albicans* shows skew right distribution, but the few cells on the right could be due to multiple cells passing the sensing zone at once. The drug treated cell distribution shows a bimodal distribution (two peaks). The non-viable cells show an almost symmetrical distribution, and the cells on the far right could be due to several instances of multiple cells passing the sensing zone. As discussed previously, the permeable cell population resulting from heat shocking is slightly smaller than the corresponding viable cell population. So, a larger ρ is expected for viable cells.

While ρ diagram can be affected by multiple cells passing at once, θ diagram shows reasonable results. Viable cells show a skew left and non-viable cells show a skew right distribution, and this agrees with *C. tropicalis* observation above. A bimodal distribution is seen for drug treated cells, and this could be indicative of the presence of at least two subpopulations of *C. albicans* that differ distinctly in their MICs to CSP [24].

V. Discussions and Conclusion

The obtained results show cell permittivity $\Delta\varepsilon(\Delta\varepsilon', \Delta\varepsilon'')$ or $\varepsilon(\rho, \theta)$ is likely a new trait for cell heterogeneity study. Nevertheless, there are many issues that need significant further work to address. For instance, cell shape induces $\varepsilon(\rho, \theta)$ change as discussed in [25] as well. The above discussions did not consider such cell properties, which also constitute cell heterogeneity. Clearly, future work is needed to clarify ε-based MCPV and cell shape variation. Additionally, to understand and clarify the biological significance of the obtained ε-heterogeneity is a difficult challenge. For example, it seems that viable *C. tropicalis* in Fig. 7(a) has two subpopulations since cells with $\Delta\varepsilon''<0.4$ or $\Delta\varepsilon''>0.4$ have different population MCPs. Drug treated *C. albicans* in Fig. 8(a) shows subpopulations that are drug resistant, drug tolerant and drug susceptible. Nevertheless, the observations need to be verified with biochemistry methods.

The argument for separating QMV and MCPV implies that angle α in Fig. 2 is likely cell type/species dependent since cell MCP is considered conserved for a given cell species. Such MCP conservation is the foundation for label free cell identification with Raman spectroscopy and mass spectroscopy, which has become a new standard method in microbiology laboratories. However, α value at a single frequency alone is unlikely cell type/species specific. Instead, a collection of α over a wide frequency range may enable cell species identification.

In summary, a microwave flow cytometer was built to accurately measure the permittivity values of single and nonbudding *C. tropicalis* and *C. albicans* (separately) in flow. The obtained cell permittivity values, $\Delta\varepsilon'$ vs $\Delta\varepsilon''$, is used as a new cell trait for heterogeneity investigation. Visual observations and microscope imaging analysis indicate that $\Delta\varepsilon$ heterogeneity is mainly due to the variation of molecular quantities, not molecular composition profile, in cells. Therefore, it is reasonable to separate cell heterogeneity into QMV and MCPV to help understand cell population characteristics. Measured drug-treated *C. tropicalis* and *C. albicans* show significantly increased heterogeneity. Thus, high throughput microwave measurement of single cells is promising to be a non-invasive and label-free technique for cell heterogeneity characterization and screening. It complements currently available "omics" and other methods. Nevertheless, significant work is needed to simultaneously obtain multi-frequency $\Delta\varepsilon(f)$ of cells in a population and clarify the biological significance of $\Delta\varepsilon(f)$ based cell heterogeneity, among others.

REFERENCES

[1] S. Huang, "Non-genetic heterogeneity of cells in development: More than just noise," *Development*, vol. 136, no. 23, pp. 3853–3862, 2009.

[2] T. Krieger and B. D. Simons, "Dynamic stem cell heterogeneity," *Development*, vol. 142, no. 8, pp. 1396–1406, 2015.

[3] D. P. Tabassum and K. Polyak, "Tumorigenesis: It takes a village," *Nature Rev. Cancer*, vol. 15, no. 8, pp. 473–483, 2015.

[4] E. Papalexi and R. Satija, "Single-cell RNA sequencing to explore immune cell heterogeneity," *Nature Rev. Immunol.*, vol. 18, no. 1, pp. 35–45, 2018.

[5] A. H. Gough et al., "Identifying and quantifying heterogeneity in high content analysis: Application of heterogeneity indices to drug discovery," *PLoS One*, vol. 9, no. 7, 2014, Art. no. e102678.

[6] A. Wilson, M. Hodgson-Garms, J. E. Frith, and P. Genever, "Multiplicity of mesenchymal stromal cells: Finding the right route to therapy," *Front. Immunol.*, vol. 10, 2019, Art. no. 1112.

[7] M. Blanco-Calvo, Á. Concha, A. Figueroa, F. Garrido, and M. Valladares-Ayerbes, "Colorectal cancer classification and cell heterogeneity: A systems oncology approach," *Int. J. Mol. Sci.*, vol. 16, no. 6, pp. 13610–13632, 2015.

[8] K. M. Turner, S. K. Yeo, T. M. Holm, E. Shaughnessy, and J.-L. Guan, "Heterogeneity within molecular subtypes of breast cancer," *Am. J. Physiol. Cell Physiol.*, vol. 321, no. 2, pp. C343–C354, 2021.

[9] H. Zheng et al., "Single-cell analysis reveals cancer stem cell heterogeneity in hepatocellular carcinoma," *Hepatology*, vol. 68, no. 1, pp. 127–140, 2018.

[10] W. Fang et al., "Intratumoral heterogeneity as a predictive biomarker in anti-PD-(L) 1 therapies for non–small-cell lung cancer," *Mol. Cancer*, vol. 20, no. 1, pp. 1–6, 2021.

[11] S. B. Lim et al., "Addressing cellular heterogeneity in tumor and circulation for refined prognostication," *Proc. Nat. Acad. Sci. USA*, vol. 116, no. 36, pp. 17957–17962, 2019.

[12] A. Gough et al., "Biologically relevant heterogeneity: Metrics and practical insights," *SLAS Discov.*, vol. 22, no. 3, pp. 213–237, 2017.

[13] J. Grote, D. Krysciak, and W. R. Streit, "Phenotypic heterogeneity, a phenomenon that may explain why quorum sensing does not always result in truly homogenous cell behavior," *J. Appl. Environ. Microbiol.*, vol. 81, no. 16, pp. 5280–5289, 2015.

[14] R. A. Rocha, J. M. Fox, P. G. Genever, and Y. Hancock, "Biomolecular phenotyping and heterogeneity assessment of mesenchymal stromal cells using label-free Raman spectroscopy," *Sci. Rep.-U.K.*, vol. 11, 2021, Art. no. 4385.

[15] F. Artis et al., "Microwaving biological cells: Intracellular analysis with microwave dielectric spectroscopy," *IEEE Microw. Mag.*, vol. 16, no. 4, pp. 87–96, May 2015.

[16] S. Afshar, E. Salimi, K. Braasch, M. Butler, D. J. Thomson, and G. E. Bridges, "Multi-frequency DEP cytometer employing a microwave sensor for dielectric analysis of single cells," *IEEE Trans. Microw. Theory Techn.*, vol. 64, no. 3, pp. 991–998, Mar. 2016.

[17] A. Tamra, D. Dubuc, M.-P. Rols, and K. Grenier, "Microwave monitoring of single cell monocytes subjected to electroporation," *IEEE Trans. Microw. Theory Techn.*, vol. 65, no. 9, pp. 3512–3518, Sep. 2017.

[18] H. Li, X. Ma, X. Du, L. Li, X. Cheng, and J. C. Hwang, "Correlation between optical fluorescence and microwave transmission during single-cell electroporation," *IEEE Trans. Biomed. Eng.*, vol. 66, no. 8, pp. 2223–2230, Aug. 2019.

[19] J. A. Osterberg et al., "Microwave sensing of yeast cell species and viability," *IEEE Trans. Microw. Theory Techn.*, vol. 69, no. 3, pp. 1875–1886, Mar. 2021.

[20] N. Dahal et al., "Spectroscopic analysis of candida species, viability, and antifungal drug effects with a microwave flow cytometer," *IEEE J. Electromagn., RF Microw. Med. Biol.*, vol. 6, no. 4, pp. 566–573, Dec. 2022.

[21] N. Heintz and S. Gong, " Small-scale preparations of yeast DNA," *Cold Spring Harb. Protoc.*, vol. 2020, no. 10, pp. 430–432, 2020.

[22] V. Letscher-Bru and R. Herbrecht, "Caspofungin: The first representative of a new antifungal class," *J. Antimicrobial Chemotherapy*, vol. 51, pp. 513–521, 2003.

[23] S. Silva, M. Negri, M. Henriques, R. Oliveira, D. W. Williams, and J. Azeredo, "Candida glabrata, candida parapsilosis and candida tropicalis: Biology, epidemiology, pathogenicity and antifungal resistance," *FEMS Microbiol. Rev.*, vol. 36, pp. 288–305, 2012.

[24] S. Schwarz et al., "Editorial: Assessing the antimicrobial susceptibility of bacteria obtained from animals," *J. Antimicrobial Chemotherapy*, vol. 65, pp. 601–604, 2010.

[25] A. D. Biasio, L. Ambrosone, and C. Cametti, "The dielectric behavior of nonspherical biological cell suspensions: An analytic approach," *Biophys. J.*, vol. 99, pp. 163–174, 2010.